Journal of Metals, Materials and Minerals, Vol. 30, No. 4, pp. 1-18, 2020

Magnetic sensors and geometrical magnetoresistance: A review

Abdelfattah Mohammed MANSOUR[1,2,*]

[1] *Solid State Physics Department, Physics Research Division, National Research Centre, Dokkii, Cairo 12622, Egypt*
[2] *Center of Microelectronics in Provence, Mines Saint-Etienne, F-13541 Gardanne, France*

***Corresponding author email:** ae.mansour@nrc.sci.eg, mailto:amamansour@gmail.com

Received date:
8 June 2020
Revised date
21 September 2020
Accepted date:
13 October 2020

Keywords:
Magnetic;
Sensor;
Geometrical;
Extraordinary;
Magnetoresistance

Abstract

Magnetic sensing devices are of the extremely significant kind of detectors, that are used several important and useful applications. Geometrical extraordinary magnetoresistance (EMR) is the geometrical kind of magnetoresistance associated with the non-magnetic semiconductor-metal hybrid structure and influenced by geometrical shape. As a result of Lorentz force, the current path change from metal (in absence of magnetic field) to semiconductor (under the subjection of the magnetic field) in semiconductor-metal hybrid structure is the key of EMR phenomena, i.e. once the metal is placed in a semiconductor, it works as a short circuit with the majority of applied current moving through metallic inhomogeneity and the almost whole resistance of semiconductor-metal hybrid structure drops to value smaller than that of homogeneous semiconductor in absence of magnetic field, in other hands, applying of magnetic field alters the current route to be around the metallic inhomogeneity where it works as an open circuit and the whole resistance turns into a quite high magnitude relies on the geometrical form of a device. The variables govern these phenomena are metal and semiconductor conductivity, semiconductor charge carriers mobility, and device geometry. Within this review, EMR phenomena history, variables governed it, materials, and applications of EMR devices are overviewed.

1. Introduction

In our day-to-day life, we frequently use different types of sensors in several applications such as IR sensor used for operating television remote, Passive Infrared sensor used for automatic door opening system of shopping malls, and light-dependent resistor (LDR) sensor used for outdoor lighting or street lighting system [1-5]. Sensors have become in the present day a basic necessity in industrial applications, they are considered as members of the senses of the control system and without the control system is unable to have it be independently publicly outside the center and controlled system changes [6-12]. Where the worker is the source of all information about the treatment process and was on the worker to know whether there is a spare available, or any of the pieces were ready, and is it valid or corrupt, and whether the tools in good condition, and does Where to install open or closed, and so on. and therefore, it was incumbent on the worker to his own fumbles problems in the production process. But, primarily we must know what a sensor is. The word sensor comes from a Latin origin "sentire," which refers to "to perceive," started in 1350-1400, the Middle British period [5]. A sensor is a tool usually senses and replies to variations of an event located in surrounds. An event could be a magnetic field, light, pressure, motion, heat, moisture, or any other external events [13,14].

The transducer is the other term that is sometimes interchangeably used instead of the term sensor although there are delicate differences. A transducer is a device that turns one type of energy into another [15] through the thermal or chemical transitions [16]. The origin is "transduce," meaning "to transfer" that was initially coined in 1525-1535. A concept of the transducer is often utilized for the meaning of many types of equipment including sensors, junctions, or actuators [5]. A schematic diagram of the sensor is depicted in Figure 1. A sensor is usually manufactured from two major components: a sensitive element and a transducer. The sensitive element can interact with an objectively measured and create a change in the functions of the transducer.

Under suffering from this change, the transducer generates a signal which is translated into readable information with a data acquisition system. It's essential to notice that for devices such as transistors and actuators, the conversion process efficiency is generally an important factor. However, besides the conversion efficiency, a sensor must have many other characteristics such as selectivity and sensitivity [15]. The expressed word sensor, on other common definitions, can be used for the sensing element itself and transducer for the sensing element plus any associated peripherals (the entire system). For example, a temperature sensor has named a sensor, while the data acquisition circuit is named a transducer. Sensors allow systems to interact with the surrounding environmental conditions and receive the desired information. This information is then delivered to a processing system, where it is prepared into magnification.

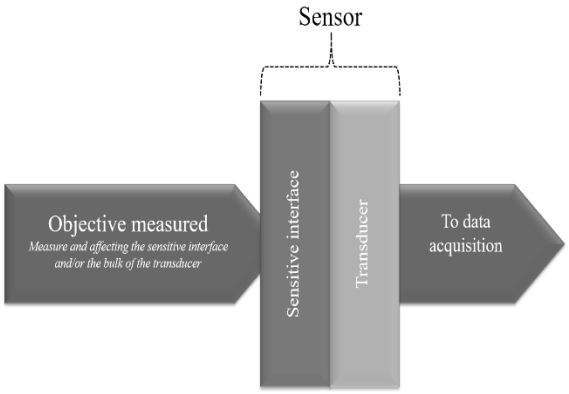

Figure 1. Schematic depiction of a sensing system.

2. Transducers types

Because the conversion of energy from form to another is a significant feature that affects the sensing operation, it will be important to know different types of energy. The list of different types of energies is presented in Table 1 [17]. Physical and chemical effects are involved in signal transductions. Physical effects contain the ones that are related to a material's thermal, mechanical, electromagnetic (including optical), gravitational, and nuclear properties. These effects together with the chemical effects are used within sensors. Various kinds of sensors are known including flow, force, pressure, humidity, motion, and more others. This review will make focusing on magnetic sensors.

Table 1. Various forms of energies and their occurrence.

Type of energy	Occurrence
Gravitational	Gravitational attraction
Mechanical	Motion, displacement, mechanical forces, etc.
Thermal	Thermal energy of an object increases with temperature. In thermodynamics, thermal energy is the internal energy present in a system in a state of thermodynamic equilibrium because of its temperature
Electromagnetic	Electric charge, electric current, magnetism, electromagnetic wave energy (including the high frequency waves such as infrared, visible, UV, etc.)
Chemical	Energy released or absorbed during chemical reactions
Nuclear	Binding energy between nuclei-binds the subatomic particles of a matter

3. Magnetic sensors

The life on earth is associated with magnetism where the gravity that enables living creatures to live on the ground and perform the different activities in a stability and steadiness state. With the increasing of industrial activities and an attempt to exploit the natural forces and the importance of controlling it, the need for sensors, at general and to magnetic sensors, in particular, appeared.

Magnetic sensors have many and many uses in various fields. Not without human activity than relying on magnetic sensors. Sensors that monitor properties like temperature, pressure, strain, or flow provide an output signal that is directly associated with the required parameter. The magnetic fields may consequently hold details on properties as direction, rotation, presence, angle, or electrical currents which can be transformed into an electrical voltage by the magnetic sensor. A few of magnetic sensors measure magnetic fields absolutely, like earth field in compass. The resulted signal needs some processing to transform into the wanted parameter.

A magnetic field distribution depends on distance and the form of disturbing target (i.e., magnet, current, etc.) or event. Hence, it is necessary often to consider both the sensor and the target in practical designing. Even though magnetic sensors are relatively more difficult to usage, they give accurate and trusted data without physical contact.

For several decades, magnetic sensors provide humans the ability to analyze, organize, and control many processes and functions. Computers have unlimited memory and can store and read information through the magnetic sensors in hard drives and write-reading heads [18]. Aircrafts flying in the sky with high safely through the magnetic controllers and magnetic sensing devices [2,3,19]. In cars, where magnetic sensors are used to determine the faults, organizing, and controlling the number of engine operations and other parts of the car [20-23]. Increase the productivity of the factories through dependence on magnetic sensors to control and regulate the production processes and quality in various industries [3,4].

4. Magnetic sensors types

A lot of methods for sensing magnetic fields are noted. Most of these methods depend on the correlation between magnetism and electricity. The magnetic sensor technologies use numerous physical phenomena. The majority of the most regular magnetic sensing techniques are stated in Figure 2.

Magnetic sensors (magnetometers) are scalar or vector sensors. Magnetometers that measure just the strength or direction are called scalar (total field) sensors, whereas that measure both are called vector magnetometers [24]. Today, both scalar and vector magnetometers are commonly found in consumer electronics, such as mobile phones, tablets, and cellular devices.

Magnetic sensor	Detectable field range			
	1 nT	1 μT	1 mT	1 T
Squid	<----------	----------	---------->	
Fiber-optic	<----	----------	------->	
Optically pumped	<------	----------	------->	
Nuclear precession	<----	----------	---------->	
Search coil	<----------	----------	----------	---------->
Earths field		<--->		
AMR sensors	<-	----------	----->	
Flux-gate	<------	----------	->	
Magnetotransistor			<----------	----->
Magneto-optical			<----	------->
Hall-effect			<----	---->
GMR sensor		<----------	----------	------->

Figure 2. Approximate sensitivity range of different magnetic field sensors.

4.1 Scalar (or total field) sensors

Scalar magnetometers are that measure only the value of the field passing the sensor without any data of the direction. Scalar magnetometer relies on the separating of spinning levels of some electrons or nucleus is proportional [24-26].

High sensitivity scalar magnetometer needs to using narrow lines resonances with long lifetimes. These types of lines limit frequency selection. Therefore, the sensitivity of these magnetometers reduces immediately for frequencies over 10 Hz [26]. Some of the scalar sensors will be discussed as follows:

4.1.1 Optical pumped scalar sensor

The optical pumped (Cesium vapor) sensor is presented in Figure 3, is based on the Zeeman Effect. Where some of the characteristic spectral lines of some atoms are split into two or more lines differ slightly in wavelength when placed in a magnetic field. This phenomenon is evident in the atoms of the alkaline elements such as cesium and rubidium [27,28]. The optical pumped sensor employs the existing three energy states of cesium's valence electron, i.e. two lower states and one higher state. The energy difference between the two lower states refers to a microwave or a radio-frequency, and the transition between one of the lower and the higher state refers to a spectral line in the optical region [29,30].

The two lower states energy difference is due to an electrons spin axes orientation difference. Concerning an applied field, subjected parallel or antiparallel orientation of electron's spin axis can be taken. The lower energy states are different in one quantum unit of spin angular momentum. The higher state is a special one chosen because it has the same angular momentum as one of the lower states. When a cesium vapor is pumped optically with light, the angular momentum of atoms changes by one unit due to photons absorption [24-26]. Consequently, electrons with energy differs from the higher state by angular momentum unit will absorb photons, but such others in the energy state with a similar angular momentum as the higher state will not. Since some photons are absorbed, the light beam becomes dim. A higher state electron drops down to one of the two lower states instantly. at each of these electron transitions, there is a probability that it will drop back to the state that cannot absorb light. Considering enough time, almost all of the electrons will drop back to the same state. At this stage, the vapor will be quite transparent to light and reported to be pumped [24-26].

Whenever a correct radio-frequency field is employed parallel to the direction of light, it will turn over the electrons and varying the spin angular momentum of the electrons. Essentially, the radio-frequency field causes electrons to transfer from one of the lower energy states to the other, reversing the optical pumping. Consequently, the vapor absorbs light again. The radiofrequency and optical effects combine to give a particularly well-defined resonance, and it is this resonance the optically pumped magnetometer intrusions [26]. The needed energy to turn electron spins, and consequently the radio frequency, varies by the magnetic field value. A response loop regulates the radio frequency to keep the lowest light transmission. The frequency, as a result, acts as a measure of the magnetic field. The optical pumped sensor detects the scalar field even though its direction [31]. Optically pumped magnetometers are fairly costly and expensive high power. Its sensitivity is high because the absorption lines are narrow due to the long relaxation times of the spins. However, these long relaxation times limit the frequency response. An additional difficulty is that the signal becomes very small when the field is oriented in some directions which are called dead zones. This problem is got over by using several sensors with several orientations for their light-pumping beams [29-32]. Currently, these types of devices are reasonably limited due to their expense and size of the glass tube keeping the alkali gas.

4.1.2 Nuclear-precession magnetometer

The magnetometer, described in Figure 4(a), makes use of the response of the nuclear moments of atoms in a hydrocarbon fluid such as benzene to a magnetic field. The Bohr magnetron $(eh/2\pi m)$ set the atomic and nuclear moment's scale, where (e) is the electronic charge, (h) is Planck's constant, and (m) is the mass [33].

Since nucleus mass is greater than the electron's mass, nuclear magnetic moments are much smaller than the electronic one. The uniform magnetic field produced by a coil current is often quickly arranging the protons in a fluid. After the polarizing current is turned off, the protons will start affected by the magnetic field. The proton spin axis which is not in positioning with a constant magnetic field tack a circular path regarding the field. The rate at which this circular path is token (i.e. precession frequency) is relative to the magnetic field strength. As a result, the processing protons create a signal in the coil whose frequency is proportional to the magnetic field strength. The nuclear-precession detector measures the scalar field. A sensor overview is seen in Figure 4(b).

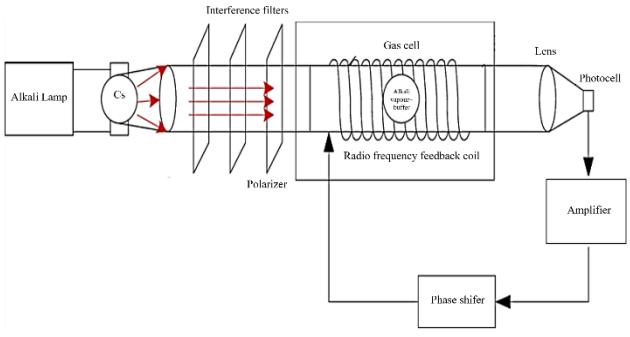

Figure 3. Diagram of optically pumped magnetometer.

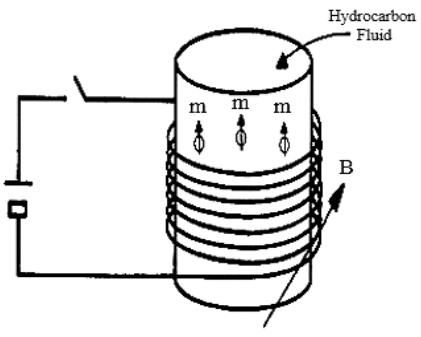

Figure 4. Diagram of Nuclear precession magnetometer.

4.1.3 Overhauser magnetometer

The overhauser effect is established on the same nuclear physics phenomena, even though partially additional complicated and again macroscopically designed to increase "simple" proton precession effects to be able to obtain much greater precession impulses from smaller sensors and employing low power [34]. Overhauser expected that, in the nuclear polarization, an increase by a factor of 1000 can be obtained by saturating the electron spin resonance. This increase tack place throughout the interaction between the proton and electron spins by means hyperfine which proportional to the vector product of electron and nuclear spins [35]. For Overhauser sensors, a liquid which contains free radical and protons is employed. Free radical is an atom that includes an individual unpaired electron, hence it is unstable chemically. They've got an electron resonant with extremely narrow line widths, about 1 Oe or nT [36]. A narrow width line enables electron resonance saturation conditions to be achieved, and consequently, increases the proton polarization with low power consumption. Frequency involved with proton precession is relative to the field which is detected through this precession frequency. At 1 Hz, noise levels of 0.015 nT/rt Hz can be accomplished by overhauser magnetometers. Its sensitivity is a magnitude order more than that involved with proton precession detectors and has not a dead region [37].

4.2 Vector magnetometers

Vector sensors are influenced by many troubles. First of all, noise troubles [38], especially frequency (*1/f*) noise [39]. Rotational vibrations are an additional main issue influence vector magnetometers.

Now we will review the different types of vector magnetometers then focus on the geometrical extraordinary magnetoresistance type.

4.2.1 Search-coil magnetometer

Induction sensors (search coil detector), based on an inductive coil, is a detector that senses the changing of magnetic flux. It is a vector sensor which detects the field value and the direction. The induction sensor can detect fields from milliHertz up to hundreds of MegaHertz [40]. Faraday's induction law stands behind induction coil magnetometers. A voltage is produced between a coiled conductor ends in case of changing the magnetic flux through it. This flux will change in three cases, case of a coil motion through a non-uniform field, case of a coil in a varying field, or a case of a uniform field with a rotating coil in it. Commonly, a high permeability ferromagnetic piece [13,14,41] is placed inside the coil to collect the encircling fields and enhance the flux density [42,43]. The core material permeability, the coil area, the turns number, and the magnetic flux change rate through the coil are the main factors that affect the magnetic field detection process by using a search-coil magnetometer [44]. Search-coil sensors can detect fields 2×10^{-5} nT, and there is no upper limit to their sensitivity range. Figure 5 shows a real search-coil magnetometer called proximity sensor and Figure 6 shows three designs for coils using in metals existence detection. These designs are resonant circuit design, bridge design, and single-coil design.

Figure 5. Real search-coil magnetometer (proximity sensor) used in metal detection.

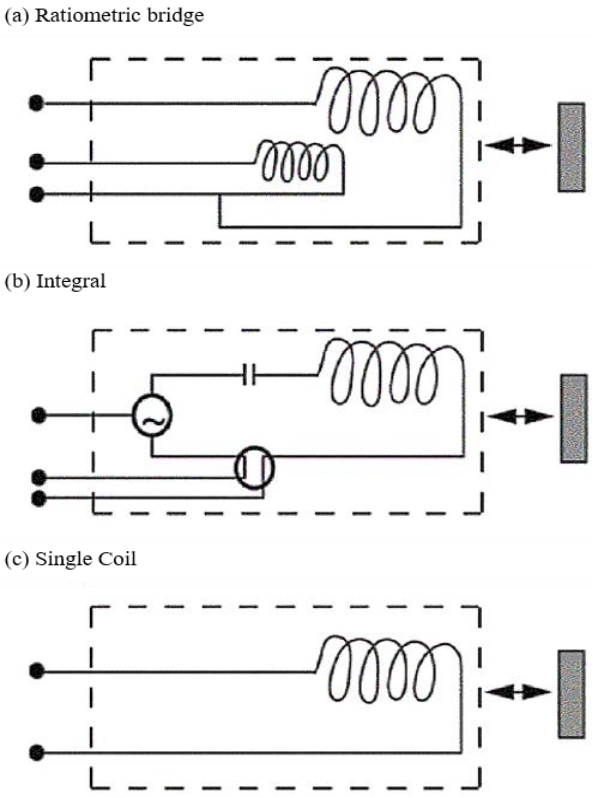

Figure 6. Schematic diagram represents three classes of proximity sensors for metals detection: (a) resonant circuit design, (b) bridge design, and (c) single-coil design.

4.2.2 Fluxgate magnetometer

It measures the level and direction of flux magnetic lines. The fluxgate magnetometer is constructed of a ferromagnetic center surrounded with two wire loops in an arrangement similar to a transformer [45]. The alternating current (AC) is moved through a primary coil which creates a varying magnetic field that produces an induced current in the secondary coil, Figure 7. The intensity and phase of the induced current in the secondary coil are continuously measured. A change of exterior field generates a change in the output secondary coil. The change level and period are employed to evaluate flux lines level and direction. A real fluxgate magnetometer is shown in Figure 8. Fluxgate magnetometers look like the search-coil magnetometers in size, but they use about five times more power. The main benefit of fluxgate magnetometers over search coils is their ability to measure direct current (DC) fields. The sensitivity range is from 10^{-2} to 10^{7}nT.

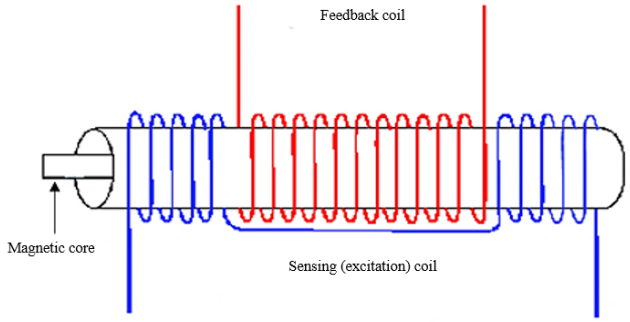

Figure 7. Schematic figure of primary and secondary coils used in fluxgate magnetometer.

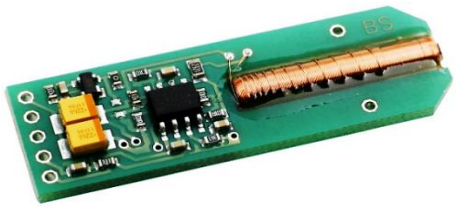

Figure 8. Real image of fluxgate magnetometer.

4.2.3 Superconductor magnetometers

4.2.3.1 SQUID sensors

The superconducting quantum interference device (SQUID), illustrated in Figure 9, is the most sensitive of all measuring magnetic field devices at low frequencies (1 Hz) [46,47]. It is depending on the interactions of electric currents and magnetic fields observed in superconducting materials below its critical temperature, at which resistance vanishes. Current will be generated and maintained its flowing forever in a superconducting ring in case of magnetic flux passing it, and this current magnitude is an indicator of magnetic flux.

In a SQUID, the regular variations are taken to evaluate the upper conducting ring current and, therefore, the enclosing magnetic field. The high sensitivity of SQUIDs enables them to be employed in medical [48], geological [49,50], astronomy applications [51,52].

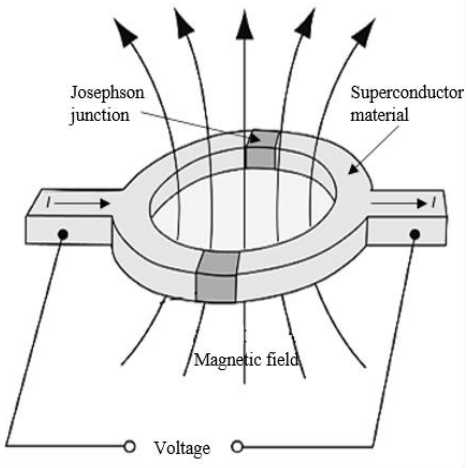

Figure 9. Schematic of SQUID.

4.2.3.2 Using the Meissner effect

Meissner's effect is a magnetic induction lines ejection from bulk superconductors interior when it cooled under their critical temperature [53], Figure 10.

The shielding current produces a field which can be measured by a low-noise giant magnetoresistance (GMR) sensor placed close to the constriction.

4.2.3.3 Spin-valve transistors

SVT is made of a semiconductor emitter, a magnetic multiple-layer base, and a semiconductor collector [54], Figure 11. The electric current passing through the SVT varies as a function of the magnetic field and this is the basis of measuring.

4.2.4 Giant magnetoimpedance (GMI) magnetic sensors

GMI is an effect that includes a huge changing of the magnetic conductor impedance when subjected to a DC. magnetic field. Experimentally, impedance is identified by the four-point technique where an AC. current passes along the sample and the voltage is used to evaluate the impedance. The two parts, real and imaginary, of impedance, lead to the GMI [55, 56].

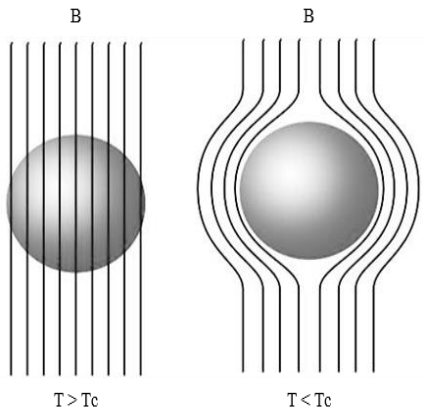

Figure 10. The Meissner effect.

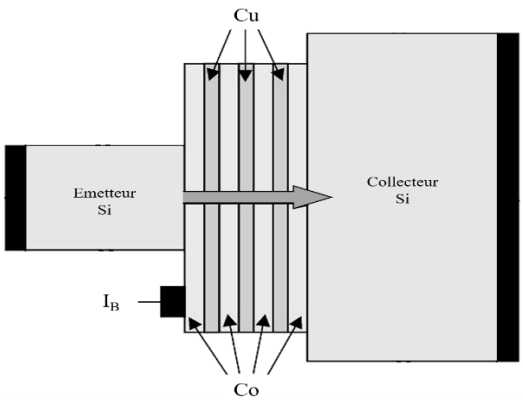

Figure 11. showing the three-terminal arrangement with semiconductor emitter (left), semiconductor collector (right), and the metallic base comprising two ferromagnetic thin layers separated by normal metals (middle).

4.2.5 Magnetodiode

Figure 12 shows a schematic representation of the magnetodiode structure, measurement sketch, and the origin of a large MR effect in p-n junction caused by spatial distribution [57]. Magnetodiode is a thin and long piece of p-i-n doped form semiconductor. The opposing surfaces of the semiconductor piece possess highly different velocities of recombination [58]. In working, the charge carriers are loaded from the n and p metal electrodes inside the i-zone and then move there under the force of the electric field E [16,59,68-77,60,78-80, 61-67]. A magnetic field normal to the charge carrier's path deflects them to down or up direction according to the field direction. Holes and electrons are displaced to the same moving direction since they are transport opposite to one another. Charge carriers near the n-type and p-type silicon interface possess a higher trend to recombination than that near the p-Si and the SiO_2 interface [81]. Therefore, in cases where the magnetic field displaces the charge carriers downward, the resistance is increased, and vice versa.

4.2.6 Magnetotransistor

Magnetotransistor shown in Figure 13, as any transistor, is made up of an n-doped emitter set aside from an n-doped collector by a p-doped base [82]. The difference is that there are two collectors instead of one. In the lack of a magnetic field, the same amounts of charge carriers reach the two collectors. in case of a magnetic field is applied perpendicular to the traveling path of the charge carriers, they are displaced closer to one of the two collectors, according to the field direction. The potential of two-collectors are provided to a difference amplifier, its outcome is relative to the subjected magnetic field [83,84].

To sense magnetic fields, Suhl and Hall's effects are used in magnetotransistors [84]. The Lorentz force, in Hall Effect, is recognized via an opposite electric field that is detected around the collectors. Suhl effect occurs once the Lorentz force is not recognized. A magnetic field within a measurement modifies the path of the transport carriers, leading to a change in the current distributions which is noticed among the collector output signals. Although the two modes happen simultaneously, systems with one main effect can be built [84].

4.2.7 Magnetostrictive magnetometers

According to the operating phenomena, there are two types of magnetostrictive magnetometers, fiber-optic and magnetoelectric magnetometer [85].

In fiber-optic magnetometer Figure14, a laser ray travels throughout a beam splitter which split it into two rays. Each ray moves along the length of one of the two fibers. These two rays are recombined and reach the photodetector at the end of every fibrous. Just one of the fibers is painted by a substance whose sizes vary with the magnitude and direction of the magnetic field [86].

In case the magnetostrictive layer is subjected to a magnetic field, the length of the coated fibrosis will change and as a result of this change, the ray moving through the fibrous reaches the detector somewhat out of phase with the ray coming from the reference one. The interference of the two rays makes the intensity level at the photodetector to vary with the phase difference. Pathway distance differences in range 10^{-13} m

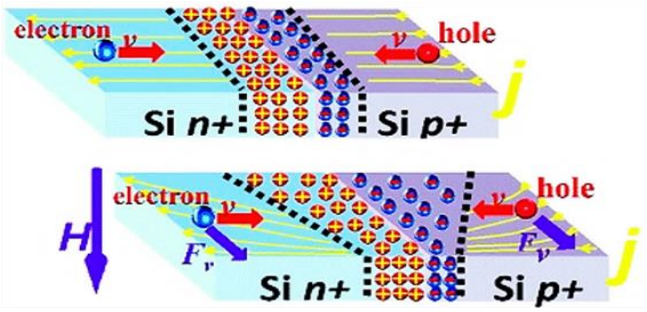

Figure 12. Schematic illustration of the origin of large MR effect in p–n junction due to the spatial distribution.

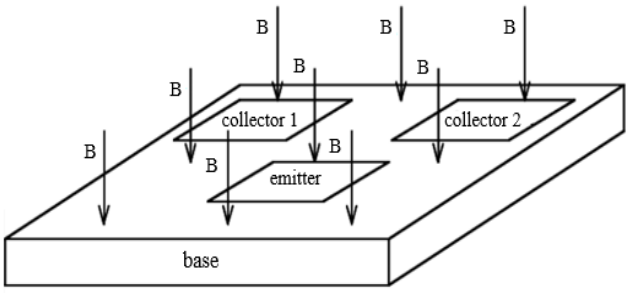

Figure 13. Drift-aided lateral double-collector magnetotransistor.

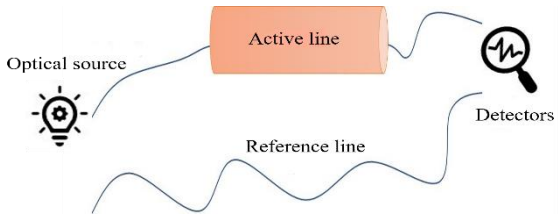

Figure 14. Fiber-optic magnetometer using magnetostrictive material.

can be recognized by the fiber-optic magnetometer. The sensor is sensible to the field lines direction and can even be used to evaluate the field lines curvature and the field strength [87].

In the other type, the magnetoelectric sensor represents the disk or plate of the magnetoelectric or piezoelectric material with two electrodes for connecting to the voltage meter [88]. The effect of the magnetic field is transferred into a voltage in the piezoelectric material. Consequently, the sensor needs no energy to create this voltage.

4.2.8 Magnetooptical sensor

The Faraday effect entails the rotation of the light polarization plane during moving throughout a magnetic material [89]. The effect is greatest in some crystals once the applied magnetic field, the crystal axis, and the light pass directions are all in-line. Linear polarized light is composed of a right and a left circular polarized beam with equal phase and frequency. Beam moving throughout a magneto-optical medium subjected to the parallel magnetic field is divided into two contra-rotating circular partial waves with different phase velocities. This behavior leads to a phase change of the two beams, even while their frequency keeps equal. The polarization plane rotation

is motived by this contra-rotating circular wave phase shift. the moment the ray leaves the MO medium, an elliptically polarized wave is produced due to the different absorption process for each of those beams. The producing signal holds the magnetic field details and consequently, evaluation of rotation angle presents the possibility to perfectly identify the magnetic field properties [90].

4.2.9 Microelectromechanical systems (MEMS) Based Magnetometers

A MEMS-based magnetic field detector is a little device used in sensing magnetic fields. Most of these sensors operate dependent on identifying the results of the Lorentz force [91]. An example of this type of magnetometers is the one based upon sensing the movement of a small magnet rod. The magnet rod reacted with the field without using any power. A MEMS-based magnetic field sensor is small in size, and so it can be placed close to the measurement position and thus maintains a more significant spatial quality [92]. Also, building a MEMS magnetic field sensor does not contain the microfabrication of a magnetic substance. Consequently, the price of the sensor could be truly lowered. Incorporation of the MEMS sensor and microelectronics can additionally lower the size of the whole magnetic field sensing system [93].

4.2.10 Hall effect sensor

Hall Effect based detectors are composed of a semiconducting thin film such as InAs, GaAs, or InSb transferring a steady electrical current along with it. Once the film is subjected to a magnetic field, the magnetic flux applies a force on the charge carrier's which in turn is deflected to the film side. Since these charge carriers are deflected sidewards, a voltage named Hall voltage is generated between the deflection sides of the film [94-100], Figure 15.

This phenomenon provides details about field value and direction. The resulted potential is directly relative to the value of the field passing subjected to the semiconductor film (output $\propto$ H).

The yield voltage is usually a few microvolts so that almost commercial Hall products are produced with an integrated amplification unite to enhance the detector resulted in a potential, level of sensitivity, and hysteresis. Also, this enables the detector to work throughout a much wider limit of field variables [91]. The resulted Hall voltage is given as:

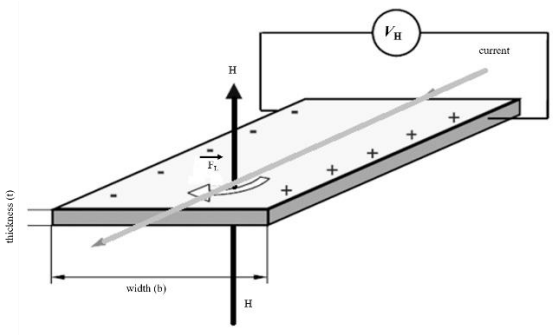

Figure 15. Hall effect sensors.

$$V_H = R_H \left(\frac{I}{t} x B\right) \quad (1)$$

Where V_H is the Hall voltage in volts, R_H is the Hall Effect coefficient in Ω·cm·G or m^3·C, I is the current flow through the sensor in Amperes, t is the thickness of the sensor in mm, and B is the Magnetic Flux density in Tesla. hall sensors give numerous of services and also a wide selection of concept illustrations.

4.2.11 Magetoresistive sensors

The substances resistivity may vary in its magnetization state. This effect is termed the magnetoresistive effect. The material magnetization will be affected by the subjection of an outward magnetic field. Therefore, the magnetoresistive effect could be employed to assemble magnetic field detecting devices. Magnetoresistance devices are highly desirable to obtain cheap products since these detectors are just empowered by employing a regular current and the resulting potential is an indicator of the measured magnetic field. Magnetoresistance (MR) is the ratio of an electrical the difference between electrical resistance in case of the subjection of the magnetic field (R_H) and absence of it (R_0), i.e. ($\Delta R = R_H - R_0$), to the resistance in no magnetic field case (R_0) [101].

$$MR = \frac{R_H - R_0}{R_0} = \frac{\Delta R}{R_0} \quad (2)$$

There are many types of magnetoresistance devices, which are established on different mechanisms of magnetoresistance, are reviewed in the next subsections.

4.2.11.1 Anisotropic magnetoresistance (AMR) sensors

The resistance change of typical magnetic metals varies with the field polarity regarding the measuring current. When the field is applied parallel to the passing electric current, the resistance raises with raising the magnetic field, and when the applied field and current are normal to one another, the resistance reduces with raising field [101]. The relative resistance difference at high fields represents the anisotropic MR effect (AMR) common to ferromagnetic metals, Figure 16. The AMR has been utilized as a PC disk head in 1990 by IBM [102].

Through the magnetization rotations in the direction of an employed field, it generally does not end up pointing to the corresponding direction as the field because its direction is recognized by several competing factors. A factor is an easy axis, the way through which the magnetization in a thin film favors to lie, which is identified by the field present during the deposition of the film. An additional factor is the film form which seems to keep the magnetization inside the crystal plane and appears to guide its position through the film length. Additionally, a crystalline anisotropy appears to guide the magnetization line up through specified plans in the crystal. Permalloy is the frequent substance used for manufacturing AMR detectors since it has got a comparatively high magnetoresistance and also for its features are agreeable by way of the manufacturing ways utilized to manufacture Si ICs [103]. Permalloy has MR less than 4%.

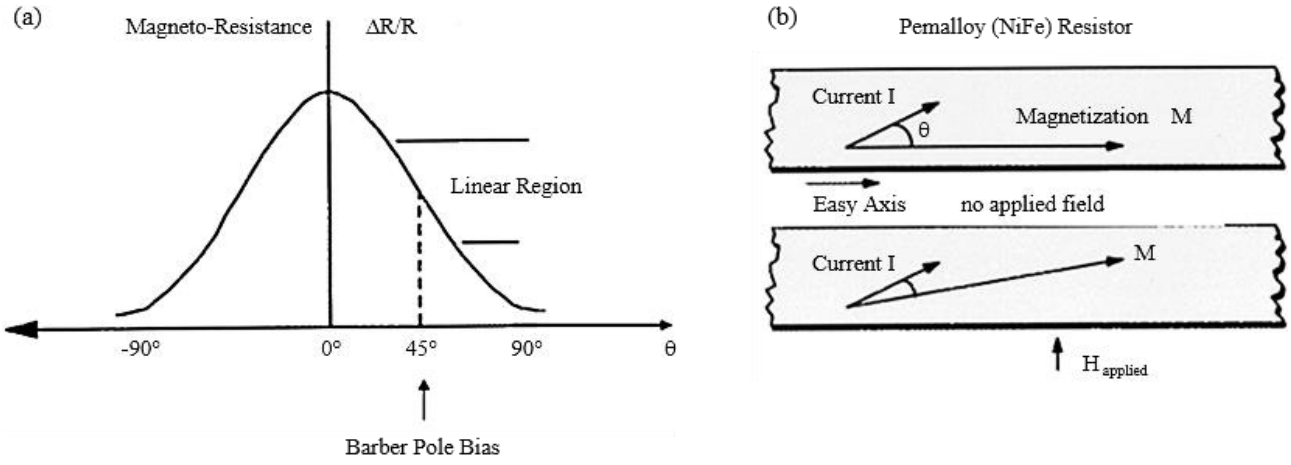

Figure 16. AMR sensor (a) change in Θ due to the application of a magnetic field and (b) resistance versus angle Θ between the magnetization and the direction of current flow.

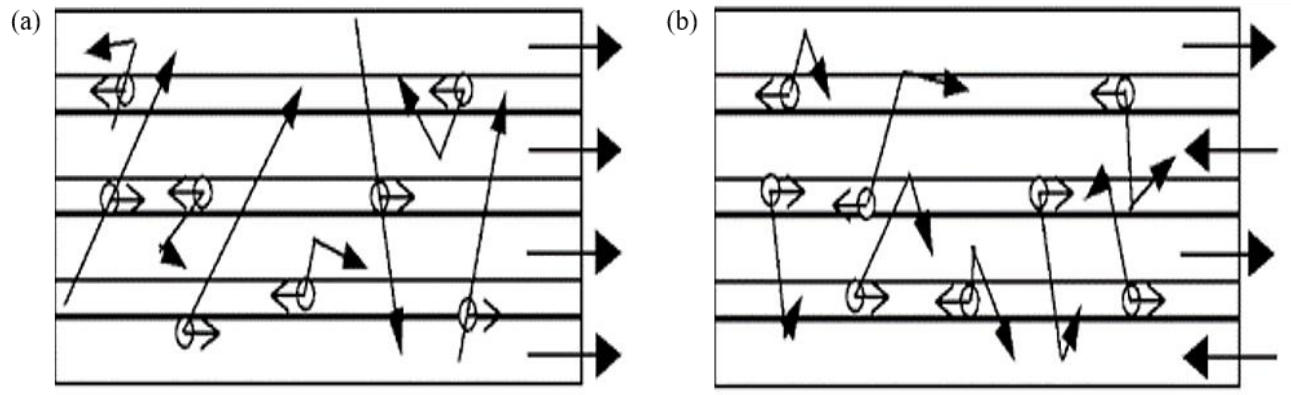

Figure 17. Schematic representation of conduction in multilayer magnetic film array, showing how differential spin scattering which produces a difference in resistance for parallel (a) and antiparallel (b) film magnetizations.

4.2.11.2 Giant magnetoresistance GMR sensors

In 1988, it was observed that MR changes as large as 50% at low surrounding temperatures in Fe/Cr multilayer structures [104]. The Fe layers were antiferromagnetically paired throughout the Cr spacer films, and the large variation in resistivity was observed stemming from the change in ferromagnetic layers relative orientation from anti-paralleling to parallel positioning as the field increases. The GM effect is schematically given in Figure 17.

GMR is obtained by a four-film arrangement which is constructed of two ferromagnets thin-film isolated by a metal. The last film layer is an anti-ferromagnetic which can prevent the magnetization rotation of one layer of the film layers [105]. Electron's motion is an ease in both parallel and normal to the films if each two layers magnetization of the ferromagnets is parallel. The explanation intended for that is as follows, in the parallel case of magnetizations, electrons undergo less scattering in the transition from an electronic band in one of the ferromagnets to the same band in another ferromagnet. The resistance difference between the two cases, magnetizations paralleling and anti-paralleling, was found to be 12.8% at room temperature [106].

The layers are needed to be highly thinner, i.e. few nanometers in thickness, to increase the effect. The primary 3 or 4 layer arrangement might be repeated to construct a multiple layers structure. This structure improves the percentage resistivity change ratio since it raises the chances of spin turn scattering through raising the interfaces in which spin turn scattering happens. In the event wherever the resistivity could be measured normal to the layer, the multilayer structure gives a greater resistivity and resistivity change. The films must be highly smooth to reduce coupling ın between the films [107,108]. GMR detectors are utilized in almost all recent pc reading heads. Figure 18 displays the way of direction change of magnetization of the 2 ferromagnetic layers with the subjection of the magnetic field. Figure 19 illustrates the change of the spin device output voltage with the applied field.

4.2.11.3 Magnetic tunnel junction sensors

Spin-dependent tunnel (SDT) detectors, or magnetically tunneling junction (MTJ), have a form like the four layers GMR detectors [109,110]. As before, two ferromagnets are isolated by an interference layer, however, in such a case the interference layer is a dielectric In MTJ detectors, the conduction arises from electrons tunneling throughout the dielectric. The dielectric layer should be highly thin and usually is Al_2O_3. Junction shorting is needed to be prevented, whether

in the manufacturing process or in unexpectedly employing an electric current throughout the junction, which produces a connection. In its simplest form, Figure 20 as an example, the MTJ is a triple-layer sandwich composed of two films of magnetic substances segregated by a thin dielectric layer [111]. If a potential is employed to the higher and lower films of this device, classical physics prevents the flowing of a current, but if the dielectric film is thin enough, electrons may cross it through the quantum tunnel effect within the dielectric layer. For the tunnel effect to tack place ın among the two magnetized layers, the maximum tunneling current will be achieved if the two electrodes magnetization directions are parallel and it will be at minimum magnitude in the case where they are antiparallel. Thus, the tunneling effect current, and also the junction resistivity, changes as subjected magnetic fields change the magnetic direction of such two layers [112].

To obtain a linearity case; the magnetization of one magnetic electrode is fixed, the other electrode is kept liberal to interact with external subjected fields. However, the pinned film layer is set by the IrMn layer that has the name pinning layer. The produced sensors possess a linear change of device resistivity with the subjected external magnetic field within a considerable range. Because of their high magnetoresistance, high impedance, and planer geometry, MTJ sensors have the potential for being used as low cost, energy-efficient, high sensitivity magnetic sensors [26].

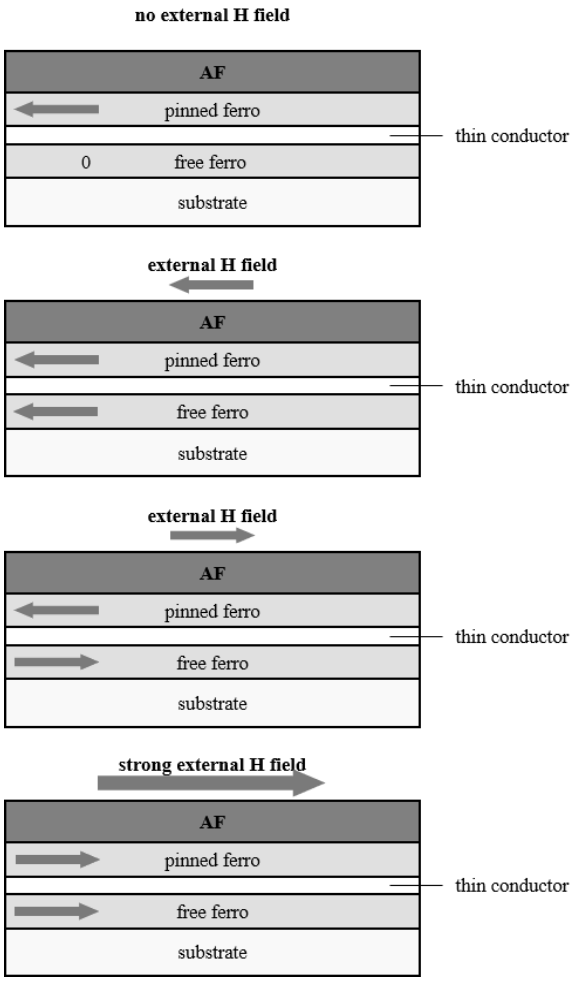

Figure 18. Orientation of the magnetization of the ferromagnetic layers in a GMR spin-valve for different external fields H.

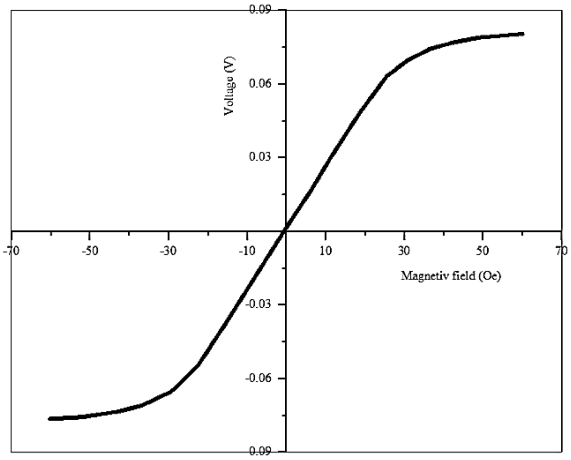

Figure 19. Voltage output versus field for a commercial spin-valve.

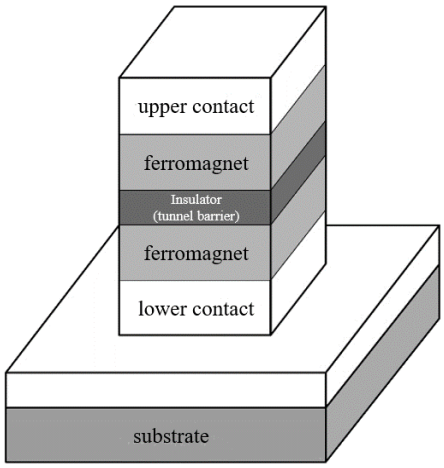

Figure 20. Schematic layer structure of a magnetic tunnel junction sensor.

4.2.11.4 Ballistic magnetoresistance

Ballistic MR (BMR) is an effect that occurs in the conduction of spin-polarized electrons through highly constricted (≈10 nm) junctions in which the spin-flip mean free path is long if compared to magnetic dominion wall width [113]. Whenever a magnetic dominion wall exists in the structure, the electrical resistivity is more than it is the value after the subjection of an external magnetic field to spread out the dominion wall. The produced magnetoresistive is higher than that of GMR or TMR. Experimentally there exists a greater change in BMR magnitude and a broad range in the conductance at which the BMR peak arises [114].

4.2.11.5 Geometrical magnetoresistance

MR may develop from the materials parameters dependence on the magnetic field or could be geometric in origin. Geometrical extraordinary MR (EMR) doesn't require magnetic substances, and comes out as a result of the Lorentz force effect on the current and potential distribution in the test sample resulting from the geometry, considering suitable boundary variables [115]. EMR is consequently related to Hall Effect. Due to variances in geometry, the Hall effect

is asymmetric in the subjection of the magnetic field, whereas the geometrical MR is symmetric. Geometries could be created resultantly of the superposition of Hall and EMR effects. The phenomena of the Hall Effect as well as the EMR have technological advantages over layered metal MR. they are not subjected to hysteresis or magnetic noise. They are not sensitive to detecting electrostatic evacuation. In semiconductors, the Hall or EMR magnitude is determined by mobility (linear and quadratic in mobility).

A great velocity process and data storing device features is accompanying with large mobility [100]. Charge carriers moving in a semiconductor within the impact of an exterior electrical field E and a normal magnetic induction B are subjected to it, as shown in Figure 21, the Lorentz force which is given with:

$$\vec{F} = q\big(E + (\vec{v}xB)\big) \tag{3}$$

Where *F* is the Lorentz force, *q* is the carriers charge, *E* is the applied electric field, $v = \mu E$ is the drift velocity of the moving carriers, μ is the carrier mobility and *B* is the magnetic field. qE is known as the electric force, while $qv \times B$ is the magnetic force F_m.

Consequently, the vector of current density *J* no longer coincides with the direction of the exterior electric field. There is an angle between *J* and *E* known as the Hall angle, which is written as:

$$\tan(\theta) = \mu_H B \tag{4}$$

Let's suppose a conductor inclusion is inserted as an inhomogeneity in a semiconductor, as seen in Figure 22. σ_s and σ_m represent a conductivities of the semiconductor and the conductor and $\sigma_m >> \sigma_s$. In the case of no magnetic field, the current moving throughout the metal where the metallic inclusion behaving as a short circuit. The current density j is parallel to the total electric field. Therefore, the direction of E and j at the semiconductor-metal interface is perpendicular to the interface (Figure 22(a)). In high magnetic fields, the Hall angle approaches 90°, in that case, j is parallel to the semiconductor-metal interface, and the current is turned around the metal inhomogeneity, which acts as an open circuit (Figure 22(b)).

As indicated, the EMR effect is a classical magnetotransport effect. So, a diffusive transport model is acceptable to represent that effect. In almost all models study the EMR, the thickness is missed and the device is regarded as two-dimensional (2D) since the thickness is very small than their planar dimensions. Moussa *et al.* [116] were firstly present a 2D reduced diffusive transport model. After that, nearly all of the simulation studies were created by utilizing simply 2D models [117-124].

Even so in certain situations when the three-dimensional (3D) current distribution is under consideration, a whole 3D transport model must be employed. Sun *et al.* [125] established a 3D model for a hybrid structure. Their result analysis was compared with practical results and found it was in good conformity with each other. Regarding Ohm's law, the current density is stated as:

$$j = \sigma(B).E \tag{5}$$

σ(B) is the tensor of magneto-conductivity which is given by:

$$\sigma(B) = ne(\mu^{-1} + B)^{-1} \tag{6}$$

where μ is the mobility and B is the magnetic field given by:

$$B = \begin{bmatrix} 0 & -B_z & B_y \\ B_z & 0 & -B_x \\ -B_y & B_x & 0 \end{bmatrix} \tag{7}$$

B_x, B_y, and B_z are the elements of the employed field in x, y, and z-directions. A 2D model is attained by missing B_x and B_y and using a normal field component B_z.

In a constant state, the identifying of electrical potential quantity $\varphi(x, y, z)$ in the hybrid structure reduces to treating of Laplace's Equation:

$$\nabla[\sigma.\nabla\varphi(x, y, z)] = 0 \tag{8}$$

The finite element approach (FE) has been employed before to treat Formula (8) within a particular boundary and primary conditions [118].

EMR effect is calculated by the use of the well-known MR relation, i.e., the change of electrical resistance in the existence of a magnetic field to the resistance at field absence, Equation (2).

The EMR sensitivity δ is identified as the resistivity change with little change, ΔB, of the field. For constant values of *I*, the sensitivity, δV, is stated with regards to the output voltage sensitivity

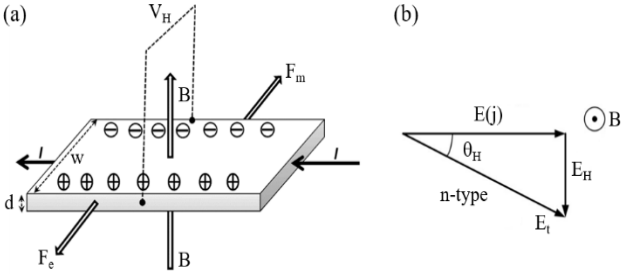

Figure 21. (a) Draw of a n-type semiconductor sheet subjected to a steady magnetic field, B, normal to the sheet surface. Employing a steady current, I will bring out charge carriers, transverse to the current path and a Hall voltage, V_H. F_m and F_e identify magnetic force and electric force. (b) Hall electric field E_H produced in an n-type semiconductor at field B. j is the current density; θ_H is the Hall angle.

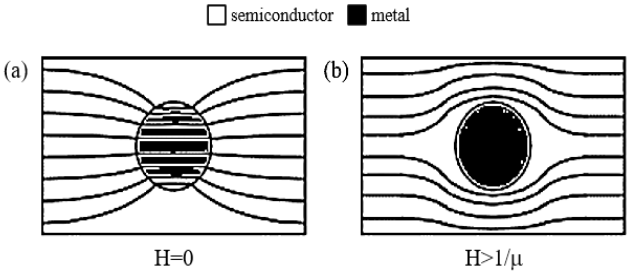

Figure 22. Current distribution in a semiconductor-metal hybrid structure. The dark lines display the paths of current. (a) At zero or poor magnetic fields, the current is parallel to the electric field E, and the metal acts as a short circuit; (b) At the high field, the current is mainly flowing in the semiconductor, the hybrid acts as an open circuit.

$$\delta(B) = \frac{R(B+\Delta B)-R(B)}{\Delta B} \xleftrightarrow{I=Constant} \frac{V(B+\Delta B)-V(B)}{\Delta B} = \delta_V(B) \qquad (9)$$

The geometry of the device is an important parameter in EMR since it is generated from the geometry of the sample. There are two major types of EMR sensors geometry, namely shunted van der Pauw- disk and shunted van der Pauw-bar Structure, respectively.

For the shunted van der Pauw-disk structure, the first geometry in it an EMR effect was discovered [115]. This geometry shape is constructed of a semiconductor disc of the radius (a) and metallic circular inhomogeneity of radius (b), Figure 23. The ratio of the radii, (α = b/a), is called the filling factor, and it has been found that α is an almost significant geometric variable in optimizing EMR magnitude [115]. For obtaining the optimum EMR effect, the ideal α value lies between 12/16 and 13/16. In such a case, EMR obtained ratios were up to 100% for fields 0.05 and 9100% for 0.25 Tesla magnetic fields. The filling factor and geometry dependence besides having been studied in several other investigations [116,126,127].

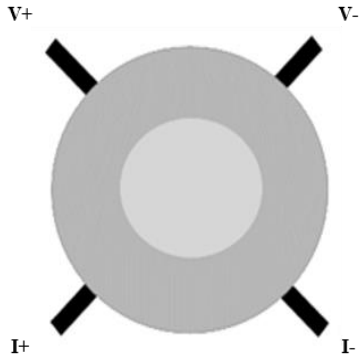

Figure 23. Sketch of the Extraordinary Magnetoresistance (EMR) devices with van der Pauw disc geometry. The dark lines labeled with I+, I−, V+, and V− represent the current leads and voltage probes, respectively. The gray blocks indicate semiconductor bulk material, and the yellow blocks indicate metal shunts.

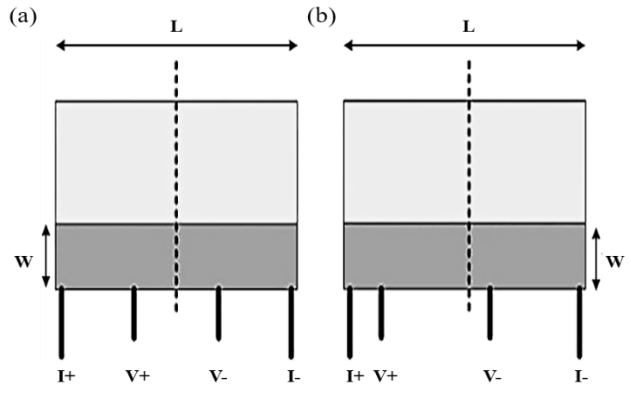

Figure 24. Sketch of the Extraordinary Magnetoresistance (EMR) devices with van der Pauw bar geometry (a) symmetric bar geometry; and symmetric bar geometry; and (b) asymmetric bar geometry. The dark lines labeled with I+, I−, V+, and V− represent the current leads and voltage probes, respectively. The dashed lines show the central axes of the bar-type devices. The gray blocks indicate semiconductor bulk material, and the yellow blocks indicate metal shunts. L is the semiconductor bar length and W is its width.

A random branch and droplet model (RBDM) [128] was applied to a vdP disk geometry. The relevance of this study result lies in its capability to be employed to EMR field detectors using more popular semiconducting substances like silicon. The model can be extended additionally with a geometry based on the microstructure of the silver chalcogenides, containing a random sized and positioned metallic braches with interspersed droplets. This model has displayed a significant and quasilinear magnetoresistance comparable to practical results. The results provided that an increase in the EMR effect of multi-branched conductor inclusion by double orders larger than geometry with a circular metallic vdP disk. To achieve a more inhomogeneity in silver chalcogenides semiconductor [129], random metallic inclusions were placed, and by using a random branch and droplet model (RBDM), a larger magnetoresistance effect, essentially an EMR effect, was reviewed. EMR effect in vdP hybrid disk was compared with that in Corbino disk with identical dimensions [130]. The EMR in the vdP disk was acquired a higher MR ratio excepting in huge magnetic fields, where the EMR effect saturates. Even so, it will be imperative to know that the large MR ratio, produced in the hybrid vdP geometry, is assigned to its smaller R(0) [115]. Therefore, although the MR ratios are extremely high, low output sensitivities can be predicted with that geometry, Equation (10). Devices of little sizes are needed to reach the appropriate spatial sensitivity and this is considered a further apparent disadvantage of hybrid vdP disk shape where troubles can be met in the manufacture of nanoscale shunted vdP disks. The dimensions announced for the first device was in the millimeter range [115] and decreased to several hundred microns in a subsequent experimental study followed that.

For the other geometrical shape, the shunted van der Pauw-bar Structure, it is a more simple construction with regards to the manufacturing process where a nanoscale EMR configuration can be obtained by using standard micro-fabrication methods [131], with an MR value of about 60% at field 0.05 Tesla is maintained. A bar-type geometry is a semiconductor-metal hybrid construction having a semiconductor bar shunted by a metal stack along one sidewall, Figure 24 [132].

Regarding the positions of the current electrodes (I) and the voltage probes (V), two forms of adjustments are usually named symmetric form and asymmetric form (Figure 26(a-b)), where the leads positions are symmetrical or asymmetrical with respecting to the bar center axis of the device, respectively. In symmetric form, the maximum MR is obtained with a voltage probes separation distance of about half of device length (L/2) [133] and decreases whenever they are pushed nearer to or even farther from each other. Low-field MR improvement was noticed for the asymmetric form [119]. An asymmetric form reveals a higher sensitivity at low fields and lower sensitivity high fields in contrast to the symmetric configuration. In both constructions, the EMR device sensitivity increases with an increase of distance between voltage probes [121]. Many types of research on the EMR were performed utilizing bar form geometry. The length over width ratio (L/W) of the semiconductor bar was noticed as an essential variable for the bar form the EMR device where the optimal EMR was achieved with L/W ≈ 20 [134-136]. The MR drops greatly when the L/W ratio reaches a value less than 20 specifically at higher fields. Furthermore, the scaling of a bar device has no bearing on the performance as

long as the ratio L/W stays the same [117]. Overlapping of voltage and current electrodes get a large sensitivity and also suggest a two electrodes EMR device with high sensitivity [117]. The resistivity and sensitivity of a simple EMR device with only two electrical contacts were reviewed within different fields and at varied temperatures [137]. Strong temperature dependence of the sensitivity was observed. The optimum value of 562 Ω·T has been found at a temperature of 75 K and a normal field of 0.26 Tesla. This form also shows planar-fields sensitivity up to 20 or 25% of the one to normal fields. These results show an influence of planar fields within the output signal of EMR sensors and additionally propose the possibility of designing an EMR form sensitive to planar fields. Using a modified form, the IVIV electrode layout (Figure 25) where the EMR effect blend with the Hall effect, leads to higher sensitivity than the asymmetric configuration [138, 139]. But, the reduced two-contact form has greater efficiency at higher fields [138].

Three contacts EMR enhancement in low-field sensitivity [140] was noticed in another construction presented in Figure 26. In this construction form, one of the voltage probes is inserted on the metal shunt rather than on the semiconductor side. A significant improvement of the resulting sensitivity has been detected at low magnetic fields compared to the ordinary EMR device, that owning to Hall Effect.

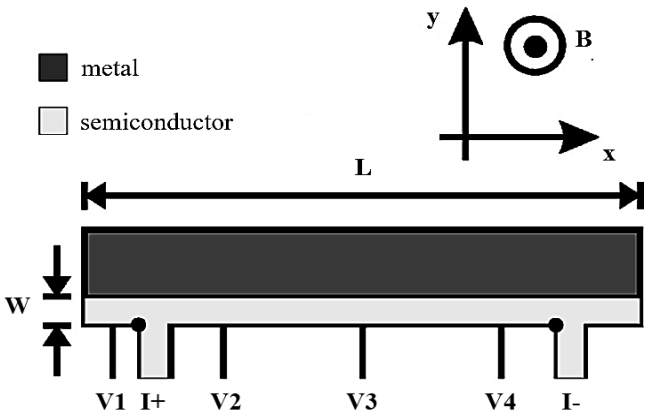

Figure 25. Sketch of the semiconductor-metal hybrid structure (top view). The current leads are labeled I+, I−, and the voltage probes are labeled V1 through V4.

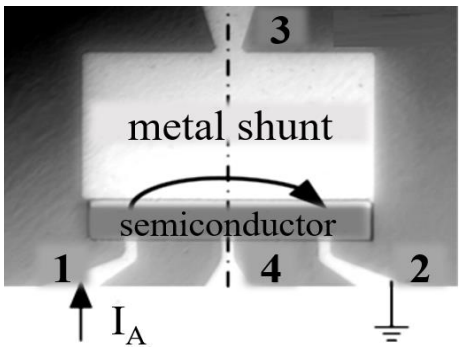

Figure 26. Optical micrograph of the EMR device. The current is injected through the electrodes labeled as 1 and 2, and the arrow shows the direction of current flow. The output signal is measured through electrodes 3 and 2. The external magnetic field is applied perpendicularly to the illustration plane.

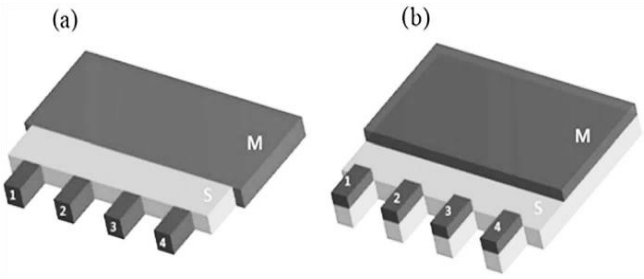

Figure 27. Geometrical forms of EMR magnetoresistors. (a) Standard 3D construction, (b) 2D (planar) construction. M is a high conductivity metal, S is a high electron mobility semiconductor and 1-4 are electric terminals.

The resulted sensitivities of 1.9 Ω·Tesla at no field and 2 Ω·Tesla at 0.01 Tesla were scored, which means that it is comparable to the common EMR detectors with a bias of ~0.04 Tesla. A five-contact construction form IVIVI was created where the current is applied by using three probs. This form showed an improvement three times higher than that of the four-contact IVIV construction form [134].

A coplanar Ag metallic shunt with the sensitive InSb semi-conductor thin film was studied [141]. This physical 2D planar form, Figure 27, will be easily made with the common thin-film industry. Another benefit is the applicability of building an EMR detector established on the high mobility electron/hole gas enclosed in the new electronic materials like graphene which is physically 2D by nature.

While the EMR phenomenon is a geometrically based effect, there is a considerable effect by the semiconductor material factors on the device functionality. The semiconductor mobility (μ_s) was found as the maximum critical variable [120]. The EMR improves with raising values of (μ_s), however, when μ_s increases, the carrier density ns decreases, saving the varying of conductivity limited. Typically, semiconductors with high mobility exhibit a stronger EMR effect and are desired for EMR detectors. Owing to its poor carrier mobility, systems based on silicon show a poor EMR, 15.3% at 10 Tesla in a device made of n-doped Si ($\mu s = 0.0065$ m^2·Vs) [142]. III-V semiconductors, as InSb or InAs, with higher mobility exhibits a huge EMR of 1000% at 5 Tesla with a polycrystalline InSb with mobility of 1.22 m^2·Vs, produced by thermal evaporation [127]. More significant mobility III-V thin films are usually manufactured by epitaxial technology. In single-crystalline InSb and InAs, mobilities of ≈7 and ≈3 m^2·Vs were detected, respectively. An EMR ratio of 750,000% at 4 Tesla and room temperature was released from an InSb thin film with thickness 1.3 μm and mobility of 4.55 m^2·Vs [115]. To generate a larger mobility value, III-V semiconducting compounds thin film thickness requires to be increasing than 1 μm in thickness. As an example, bulk InSb mobility decreases greatly to 0.01 m^2·Vs in a 0.1 μm thick film [143]. This forbids III-V thin films to be employed in sub-micron dimensions tools. Highly thin films, about 100 nm, from III-V ingredients are utilized to eliminate the poor mobility difficulty in thin bulk films. Two dimensions electron gaseous (2DEG) with high mobility could be obtained with AlSb/InAs structure (termed "6.0 Å material systems") by utilizing epitaxial growth. These structures exhibit a huge room temperature mobility beyond 2 m^2·Vs [144]. As a result of 2DEG, mesoscopic EMR appliances are now obtained. A mesoscopic IVIV EMR device was manufactured using graphene [145-147]. This device sensitivity reaches values up

to 105 mV·T, which is much greater, compared to that produced in 2DEG models. The efficiency will be configured by varying the mobility and charge carrier density of a graphene film by an electric field employed by a back-gate voltage.

Metal inclusion is also a significant factor affecting the EMR device's efficiency. It should have a great conductivity to short the semiconductor at no field. A conductivity proportion ın between conductor and semiconductor is essential to be higher than 10^6 for a massive EMR effect. The EMR effect decreases quickly when the ratio decrease under 10^5 [133]. Also, the contact conditions gained at the interface perform a significant variable. An ohmic contact having low contact resistivity is essential for the EMR devices [118]. A high contact resistivity behaves as a potential wall which eliminates current flowing into the metal shunt and hence lowering the effect. Contact resistivity from 10^{-11} Ω·cm^2 to 10^{-7} Ω·cm^2 has a constant MR ratio. For sensitivity, this range is from 10^{-11} Ω·cm^2 to 10^{-8} Ω·cm^2. Magnetoresistance ratio and sensitivity decrease with the increase of contact resistivity above 10^{-7} Ω·cm^2 and 10^{-8} Ω·cm^2, respectively. The extraordinary effect in a device with contact resistivity values 10^{-5} Ω·cm^2 is 0.4% of that of an ideal appliance. For a contact resistivity lower than 10^{-8} Ω·cm^2, the sensitivity shows a magnitude of ≈86 Ω·T. It drops rapidly to 74 Ω·T at 10^{-5} Ω·cm^2 as the contact resistivity increases.

To get good electric contact and then simplify the manufacture, different thicknesses and overlapping of semiconductor and metal shunt should be achieved. This process generates a vertical current component, which is minimal in the case of an EMR device constructed from a 2DEG but not in that produced from a bulk material [148]. This vertical component reduces the EMR effect and its sensitivity to normal fields. The outcome sensitivity is lowered by 10% if the metal shunt thickness is decreased to 20% of the semiconductor thickness [125]. Moreover, metal and semiconductor overlapping leads to sensitivity drops by about 10%. Using 2DEG produces constructions with two-dimensional transport systems, accordingly the geometry of the semiconductor/metal interface has a small effect.

5. Conclusions

The total field and the vector magnetometers are the main types of the magnetic field according to whether they measure the scalar or the vector components of the magnetic field. The most popular magnetic field detecting techniques have already been reviewed and the fundamental physical basics regulating its technique were presented. The different types presented in this review are search coil, optical, fluxgate, nuclear, SQUID, anisotropic, giant magnetoresistance, tunneling junctions, magnetoimpedance, magnetostrictive, piezoelectric, magnetodiode, magnetotransistor, Hall-effect, and geometrical extraordinary magnetoresistance (EMR). The extraordinary magnetoresistance phenomenon has been discussed in some details. In identifying the magnetotransport characteristics of extraordinary magnetoresistance structures, it was noticed that the geometry performs an important factor. Different geometrical shapes and constructions showed an extraordinary magnetoresistance appearance. Two main geometrical types, namely shunted van der Pauw-disk and shunted van der Pauw-bar Structure, respectively. The vdP disk geometry undergoes some disadvantages of low produced signal and troubles in its size. Therefore, the bar-type constructions were recommended. The efficiency of EMR systems can be altered by its electrodes positions. A small betterment was detected for asymmetric electrode arrangement. Additional improvements in low-field efficiency were observed in the VIVI construction, and a three-contact setup merging both EMR and Hall Effect. III–V materials and the 2DEG heterostructures are the best selections for EMR construction owing to their high mobility. A metallic shunt with high conductivity is desired to have a large EMR effect. Also, the semiconductor-metal contact resistivity should be under 10^{-7} Ω·cm^2. As a consequence of its drawbacks, such as the low result signal in the low field s and the nonlinearity responding, EMR devices have not strengthed in the magnetic sensor market. But, it can be estimated to happen by more studies soon.

References

[1] G.R. Tschulena, and A. Lahrmann, *Sensors in household appliances*. *Wiley-VCH*, Weinheim, 2003.

[2] I. Inasaki, and H.K. Tönshoff, *Sensors in manufacturing*. *Wiley-VCH*, Weinheim, 2001.

[3] J. Fraden, *Handbook of Modern Sensors : Physics, Designs, and Applications*., 2016.

[4] O. Gassmann, J. Hesse, and H.K. Tönshoff, *Sensors applications. 6, Environmental technology*. *Wiley-VCH*, Weinheim, 2002.

[5] K. Kalantar-zadeh, *Sensors An Introductory Course*. *Springer*, Boston, 2013.

[6] H. Yamasaki, *Intelligent sensors*. *Elsevier*, Amsterdam; New York, 1996.

[7] P. Wild, *Industrial sensors and applications for condition monitoring. Mechanical Engineering Publications*, London, 1994.

[8] B. Bhushan, and H. Fuchs, *Applied scanning probe methods II : Scanning probe microscopy techniques*. *Springer*, Berlin, 2006.

[9] R. Narayanaswamy, and O.S. Wolfbeis, *Optical Sensors : Industrial Environmental and Diagnostic Applications*. *Springer*, Berlin, 2004.

[10] H. Kopola, *Intensity-modulated fibre optic sensors for robotic, medical and industrial applications*. *Ouluensis Universitas*, Oulu, 1988.

[11] M. Hosseini, and A.S.H. Makhlouf, *Industrial Applications for Intelligent Polymers and Coatings*. *Springer International Publishing*, Cham, 2016.

[12] S. Nihtianov, *Smart Sensors And Mems. Woodhead*, S.l., 2017.

[13] A.B. Abou Hammad, A. Elzwawy, A.M. Mansour, M.M. Alam, A.M. Asiri, M.R. Karim, M.M. Rahman, and A.M. El Nahrawy, "Detection of 3,4-diaminotoluene based on $Sr_{0.3}Pb_{0.7}TiO_3/CoFe_2O_4$ core/ shell nanocomposite via an electrochemical approach," *New Journal of Chemistry*. vol. 44(19), pp. 7941-7953, 2020.

[14] N.A.A. Elkanzi, A.A.M. Farag, N. Roushdy, and A.M. Mansour, "Design, fabrication and optical characterizations of pyrimidine fused quinolone carboxylate moiety for photodiode applications," *Optik*. vol. 216, pp.164882, 2020.

[15] R.E. Newnham, "Transducers, sensors, and actuators," *Japanese Journal of Applied Physics*. vol. 25(S1), pp. 9-14, 1986.

[16] A.M. Mansour, I.M.E. Radaf, T.A. Hameed, and G.B. Sakr, "Investigation of Ag_2HgI_4 nanoparticles: Thermal phase transition and non-isothermal kinetic study," *UPB Scientific Bulletin, Series B: Chemistry and Materials Science*. vol. 81(1), pp. 134-148, 2019.

[17] Bureau of Energy Efficiency, "Basics of energy and its various forms," *General Aspects of Energy Management & Energy Audit*. no. May, pp. 38-56, 2014.

[18] J.A. Brug, T.C. Anthony, and J.H. Nickel, "Magnetic recording head materials," *MRS Bulletin*. vol. 21(09), pp. 23-27, 1996.

[19] J. Kral, "The lift-off effect in eddy currents on thickness modeling and measurement," *IEEE Transactions on Instrumentation and Measurement*. vol. 62(7), pp. 2043-2049, 2013.

[20] K. Miki and K. Masamune, "High-resolution small field-of-view magnetic resonance image acquisition system using a small planar coil and a pneumatic manipulator in an open MRI scanner," *International Journal of Computer Assisted Radiology and Surgery*. vol. 10(10), pp. 1687-1697, 2015.

[21] E. Bagalini, "Designing autonomous race car models for learning advanced topics in hard real-time system," *International Journal of Robotics Applications and Technologies (IJRAT)*. vol. 3(1), pp. 1-22, 2015.

[22] P. Xu, "Optimizing the alignment of inspection data from track geometry cars," *Computer-Aided Civil and Infrastructure Engineering*. vol. 30(1), pp. 19-35, 2015.

[23] V. Ivanov, "A review of fuzzy methods in automotive engineering applications," *European Transport Research Review : An Open Access Journal*. vol. 7(3), pp. 7-29, 2015.

[24] J. Včelák and P. Kašpar, "Sensors for vector magnetometers.," *Journal of Electrical Engineering*. vol. 57(8), SUPPL, pp. 178-180, 2006.

[25] L. Tøffner-Clausen, "In-flight scalar calibration and characterisation of the Swarm magnetometry package," *Earth, Planets and Space*. vol. 68(1), pp. 68-129, 2016.

[26] J. Lenz, and S. Edelstein, "Magnetic sensors and their applications," *IEEE Sensors Journal*. vol. 6(3), pp. 631-649, 2006.

[27] H.-C. Koch, "Design and performance of an absolute ^{3}He/Cs magnetometer," *The European Physical Journal D : Atomic, Molecular, Optical and Plasma Physics*. vol. 69(8), pp. 69-202, 2015.

[28] J.S. Markiyeh, M.R. Moniri, and A.R. Monajati, "Detection of Magnetic Anomaly Using Total Field Magnetometer," pp. 1813-1820, 2015.

[29] Z. Ding, "Optically pumped rubidium atomic magnetometer with elliptically polarized light," *Optik - International Journal for Light and Electron Optics*. vol. 127(13), pp. 5270-5273, 2016.

[30] T. Kobayashi, "Optically pumped atomic magnetometer," *The Journal of the Institute of Electrical Engineers of Japan*. vol. 136(1), pp. 26-29, 2016.

[31] D. Budker, and M. Romalis, "Optical magnetometry," *Nature Physics*. vol. 3(4), pp. 227-234, 2007.

[32] D. Budker, W. Gawlik, D.F. Kimball, S.M. Rochester, V. V. Yashchuk, and A. Weis, "Resonant nonlinear magneto-optical effects in atoms," *Reviews of Modern Physics*. vol. 74(4), pp. 1153-1201, 2002.

[33] M. Sabean, *Atomic Structure. Infobase Pub*, New York, 2011.

[34] F. Masci, "Evidence of underground electric current generation during the 2009 L'Aquila earthquake: Real or instrumental?," *Geophysical Research Letters*. vol. 43(12), pp. 6153-6161, 2016.

[35] H. Korth, "Miniature atomic scalar magnetometer for space based on the rubidium isotope ^{87}Rb," *Journal of Geophysical Research: Space Physics*. vol. 121(8), pp. 7870-7880, 2016.

[36] S. Fan, S. Chen, S. Zhang, X. Guo, and Q. Cao, "An improved overhauser magnetometer for Earth's magnetic field observation," In: J.J. Butler, X. (Jack) Xiong, and X. Gu, Eds. *Proceedings of SPIE - The International Society for Optical Engineering*. pp. 99721N (2016).

[37] V. Sapunov, "Application of overhauser DNP and K optics INTERMAGNET quantum magnetometers to fundamental physics and cosmology," *Magnetic Resonance in Solids*. vol. 18(2), pp. 1610 (4pp), 2016.

[38] A.F.M. Nor, E.W. Hill, K. Birthwistle, and M.R. Parker, "Noise in NiFeCo/Cu spin valve sensors," *Sensors and Actuators A: Physical*. vol. 81(1-3), pp. 67-70, 2000.

[39] R.J.M. van de Veerdonk, P.J.L. Belien, K.M. Schep, J.C.S. Kools, C. de Nooijer, M.A.M Gijs, R. Coehoorn, and W.J.M. de Jonge, 1/f noise in anisotropic and giant magnetoresistive elements. *Journal of Applied Physics J. M. Journal of Applied Physics*. vol. 82(12), pp. 6152-6164, 1997.

[40] A. Grosz, E. Paperno, S. Amrusi, and B. Zadov, "A three-axial search coil magnetometer optimized for small size, low power, and low frequencies," *IEEE SENSORS JOURNAL*. vol. 11(4), pp. 1088-1094, 2011.

[41] E.H. El-Khawas, A.A. Azab, and A.M. Mansour, "Structural, magnetic and dielectric properties of reduced graphene oxide/ $La_{0.9}Bi_{0.1}FeO_3$ nanocomposites," *Materials Chemistry and Physics*. vol. 241, pp. 122335, 2020.

[42] C. Coillot and P. Leroy, "Induction magnetometers principle, modeling and ways of improvement," *Magnetic Sensors - Principles and applications*. no. 1, pp. 45-64, 2012.

[43] I. Hrvoic, "Overhauser magnetometers for measurement of the Earth's Magnetic field," http://www.geophysik.uni-bremen.de/statisch/downloads/254/Overhauser-Magnetometers.pdf, 1989.

[44] S. Tumanski, "Induction coil sensors - a review," *Measurement Science and Technology*. vol. 18(3), pp. R31-R46, 2007.

[45] M. Vladislav, A. Grosz, and L. Klein, "Planar Hall Effect (PHE) magnetometers," In: A. Grosz, M.J. Haji-Sheikh, and S.C. Mukhopadhyay, Eds. *High Sensitivity Magnetometers, Smart Sensors, Measurement and Instrumentation 19*. pp. 201-224. *Springer International Publishing*, Cham (2017).

[46] K. Li and S.P. Hubbell, "High temperature superconductor transimpedance amplifiers using serially connected bi-crystal junction SQUID arrays," *IEEE Transactions on Applied Superconductivity*. vol. 9(2), PART 3, pp. 4420-4423, 1999.

[47] V. Pizzella, S. Della Penna, C. Del Gratta, and G.L. Romani, "SQUID systems for biomagnetic imaging," *Superconductor Science and Technology*. vol. 14(7), pp. R79-R114, 2001.

[48] A. Banobre, I. Padron, A.T. Fiory, and N.M. Ravindra, "Metal Diaphragm Based Magnetic Field Sensor," vol. 1, no. October 2016, pp. 693-700, 2012.

[49] H. Oda, J. Kawai, M. Miyamoto, I. Miyagi, M. Sato, A. Noguchi, Y. Yamamoto, J-ichi. Fujihira, N. Natsuhara, Y. Aramaki, T. Masuda, and C. Xuan, "Scanning SQUID microscope system for geological samples: system integration and initial evaluation," *Earth, Planets and Space*. vol. 68(1), pp. 179-198, 2016.

[50] E.A. Lima and B.P. Weiss, "Ultra-high sensitivity moment magnetometry of geological samples using magnetic microscopy," *Geochemistry, Geophysics, Geosystems*. vol. 17(9), pp. 3754-3774, 2016.

[51] K. Mitsuda, "TES X-ray microcalorimeters for X-ray astronomy and material analysis," *Physica C: Superconductivity and its Applications*. vol. 530, pp. 93-97, 2016.

[52] H. Paik, "Superconducting gravity gradiometer for sensitive gravity measurements. I. Theory," *Phys. Rev. D*. vol. 35(12), pp. 3551-3571, 1987.

[53] J.E. Hirsch, "On the dynamics of the meissner effect," *Physica Scripta*. vol. 91(3), p. 035801(15pp), 2016.

[54] Y. Xu, D.D. Awschalom, and J. Nitta, Eds., *Handbook of Spintronics*. *Springer*, Dordrecht, 2016.

[55] A. Asfour, J.-P. Yonnet, and M. Zidi, "A high dynamic range GMI current sensor," *Journal of Sensor Technology*. vol. 02(04), pp. 165-171, 2012.

[56] S.-L. Zhang, Y.-S. Chai, D.-Q. Fang, L.-C. Wang, D.-W. Xing, and J.-F. Sun, "Giant magneto-impedance effect of two paralleled amorphous microwires," *Rare Metals*. vol. 35(4), pp. 344-348, 2016.

[57] D. Yang, F. Wang, Y. Ren, Y. Zuo, Y. Peng, S. Zhou, and D. Xue, "A large magnetoresistance effect in p-n junction devices by the space-charge effect," *Advanced Functional Materials*. vol. 23(23), pp. 2918-2923, 2013.

[58] R. Popovi, and W. Heidenreich, "Magnetogalvanic sensors," In: *Sensors*. pp. 43-96. *Wiley-VCH Verlag GmbH*, Weinheim, Germany.

[59] I.T. Zedan, E.M. El-Menyawy, and A.M. Mansour, "Physical characterizations of 3-(4-methyl piperazinylimino methyl) rifampicin films for photodiode applications," *Silicon*. vol. 11(3), pp. 1693-1699, 2019.

[60] A.M. Mansour and I.M. El Radaf, "Structural, optical and electrical properties of $CuBiS_2$ thin films deposited by spray pyrolysis at different deposition times," *International Journal of Microstructure and Materials Properties*. vol. 14(5), pp. 419-431, 2019.

[61] M. Nasr, A.M. Mansour, and I.M. El Radaf, "Current transport and capacitance-voltage characteristics of Sb_2Se_3/n-Si heterojunction diode prepared by electron beam evaporation," *Materials Research Express*. vol. 6(3), pp. 036405, 2019.

[62] A.M. El Nahrawy, A.M. Mansour, A.B. Abou Hammad, and A.R. Wassel, "Effect of Cu incorporation on morphology and optical band gap properties of nano-porous lithium magneso-silicate (LMS) thin films," *Materials Research Express*. vol. 6(1), pp. 016404, 2019.

[63] A.M. Mansour, I.M. El Radaf, and G.M. Mahmoud, "Effect of deposition temperature on structural, optical and electrical properties of chemically deposited thermochromic Cu_2HgI_4 thin films," *International Journal of Microstructure and Materials Properties*. vol. 14(5), pp. 462-77, 2019.

[64] A.M. Mansour, M. Nasr, H.A. Saleh, and G.M. Mahmoud, "Physical characterization of 5′,5″-dibromo-o-cresolsulfophthalein (BCP) spin-coated thin films and BCP/p-Si based diode," *Applied Physics A: Materials Science and Processing*. vol. 125(9), pp. 2019.

[65] A.M. Mansour, E.M. El-Menyawy, and G.M. Mahmoud, "Structural, optical and galvanomagnetical properties of low cost synthesised nanostructure Cu_2S films," *International Journal of Microstructure and Materials Properties*. vol. 14(3), pp. 272-285, 2019.

[66] A.M. Mansour, "Fabrication and characterization of a photodiode based on 5′,5″-dibromo-o-cresolsulfophthalein (BCP)," *Silicon*. vol. 11(4), pp. 1989-1996, 2019.

[67] I.M. El Radaf, A.M. Mansour, and G.B. Sakr, "Fabrication, electrical and photovoltaic characteristics of CuInGeSe4/n-Si diode," *Journal of Semiconductors*. vol. 39(12), p. 124010, 2018.

[68] N. Hassan, A.M. Mansour, N. Roushdy, A.A.M. Farag, and W.G. Osiris, "Optical sensing performance characteristics of Schottky devices diodes based nano-particle disodium 6-hydroxy-5-[(2-methoxy-5-methyl-4-sulfophenyl)azo]-2-naphthalenesulfonate thin films: A comparison study," *Optik*. vol. 158(4), pp. 1255-1265, 2018.

[69] A.A.M. Farag, F.S. Terra, A. Ashery, G.M.M. Fahim, and A.M. Mansour, "Temperature dependence of J-V and C-V characteristics of n-InAs/p-GaAs heterojunctions prepared by flash evaporation technique and liquid phase epitaxy," *Indian Journal of Pure and Applied Physics*. vol. 56(3), pp. 203-209, 2018.

[70] M. Nasr, I.M. El Radaf, and A.M. Mansour, "Current transport and capacitance–voltage characteristics of an n-PbTe/p-GaP heterojunction prepared using the electron beam deposition technique," *Journal of Physics and Chemistry of Solids*. vol. 115, pp. 283-288, 2018.

[71] I.M. El Radaf, A.M. Mansour, and G.B. Sakr, "Fabrication, electrical and photovoltaic characteristics of CuInGeSe4/n-Si diode," *Journal of Semiconductors*. vol. 39(12), pp. 124010, 2018.

[72] A.M. Mansour, I.S. Yahia, and I.M.E. Radaf, "Structural, electrical and photovoltaic properties of $PbSb_2S_5$/n-Si heterojunction synthesized by vacuum coating technique," *Materials Research Express*. vol. 5(7), pp. 2018.

[73] I.M. El Radaf, M. Nasr, and A.M. Mansour, "Structural, electrical and photovoltaic properties of CoS/Si heterojunction prepared by spray pyrolysis," *Materials Research Express*. vol. 5(1), pp. 015904, 2018.

[74] A.A.M. Farag, F.S. Terra, A. Ashery, and A.M. Mansour, "Structural and electrical characterization of n-InAs/p-GaP heterojunctions prepared by vacuum flash evaporation and liquid phase epitaxy," *Optoelectronics and Advanced Materials, Rapid Communications*. vol. 11(1-2), pp. 82-87, 2017.

[75] A.M. Mansour and A.A.M. Farag, "Structural characterizations and the influence of metal work function contact for nanocrystalline 2,9-dimethyl-4,7-diphenyl-1,10-phenanthroline based devices," *Organo Opto-Electronics An International Journal*. vol. 2(1), pp. 29-35, 2016.

[76] A.A.M. Farag, F.S. Terra, A. Ashery, and A.M. Mansour, "Structural and electrical characteristics of n-InSb/p-GaAs heterojunction prepared by liquid phase epitaxy," *Journal of Alloys and Compounds*. vol. 615(12), pp. 604-609, 2014.

[77] A.A.M. Farag, W.G. Osiris, A.H. Ammar, and A.M. Mansour, "Electrical and photosensing performance of heterojunction device based on organic thin film structure," *Synthetic Metals*. vol. 175, pp. 81-87, 2013.

[78] A.A.M. Farag, A.M. Mansour, A.H. Ammar, M.A. Rafea, and A.M. Farid, "Electrical conductivity, dielectric properties and optical absorption of organic based nanocrystalline sodium copper chlorophyllin for photodiode application," *Journal of Alloys and Compounds*. vol. 513(2), pp. 404-413, 2012.

[79] A.A.M. Farag, F.S. Terra, G.M.M. Fahim, and A.M. Mansour, "Current transport and capacitance-voltage characteristics of n-InSb/p-GaP prepared by flash evaporation and liquid phase epitaxy," *Metals and Materials International*. vol. 18(3), pp. 509-515, 2012.

[80] A.A.M.A.M. Farag, A.M.M. Mansour, A.H.H. Ammar, and M.A. Rafea, "Characterization of electrical and optical absorption of organic based methyl orange for photovoltaic application," *Synthetic Metals*. vol. 161(19-20), pp. 2135-2143, 2011.

[81] A.A.M. Farag, F.S. Terra, G.M. Mahmoud, and A.M. Mansour, "Study of Gaussian distribution of inhomogeneous barrier height for n-InSb/p-GaAs heterojunction prepared by flash evaporation," *Journal of Alloys and Compounds*. vol. 481(1-2), pp. 427-433, 2009.

[82] C. Leepattarapongpan, T. Phetchakul, N. Penpondee, P. Pengpad, E. Chaowicharat, C. Hruanun, and A. Poyai, "Magnetotransistor Based on the Carrier Recombination—Deflection Effect," *IEEE Sensors Journal*. vol. 10(2), pp. 294-299, 2010.

[83] R.D. Tikhonov, "Magnetoconcentration effect on a base pn junction of a bipolar magnetotransistor," *Russian Microelectronics*. vol. 39(5), pp. 340-351, 2010.

[84] R.D. Tikhonov, "Offset voltage of an integrated magnetotransistor sensor," *Russian Microelectronics*. vol. 39(1), pp. 42-53, 2010.

[85] A.A. Higazy, H. Afifi, A.H. Khafagy, M.A. El-Shahawy, and A.M. Mansour, "Ultrasonic studies on polystyrene/styrene butadiene rubber polymer blends filled with glass fiber and talc," *Ultrasonics*. vol. 44, no. SUPPL., pp. e1439-e1445, 2006.

[86] W. Zhang, Z. Wang, W. Huang, and F. Li, "Fiber laser sensor for simultaneous acceleration and magnetic measurement," In: *2016 IEEE SENSORS*. pp. 1-3. *IEEE* (2016).

[87] R. Blue, A. Dudus, and D. Uttamchandani, "A review of single-mode fiber optofluidics.," *IEEE Journal of Selected Topics in Quantum Electronics*. vol. 22(2), pp. 380-391, 2016.

[88] M.I. Bichurin, V.M. Petrov, R. V. Petrov, Yu.V. Kiliba, F.I. Bukashev, A. Yu. Smirnov, and D.N. Eliseev, "Magnetoelectric sensor of magnetic field," *Ferroelectrics*. vol. 280(1), pp. 199-202, 2002.

[89] M. Koschny, and M. Lindner, "Accurately analyze magnetic field distribution of magnetic materials," *Advanced Materials & Processes*. no. February, pp. 13-16, 2012.

[90] M. Ghanaatshoar, and M. Zamani, "Magneto-optical magnetic field sensors based on compact magnetophotonic crystals," *Journal of Superconductivity and Novel Magnetism*. vol. 28(4), pp. 1365-1370, 2015.

[91] A. Grosz, M.J. Haji-Sheikh, and S.C. Mukhopadhyay, Eds., *High Sensitivity Magnetometers*. *Springer*, Cham, 2017.

[92] M. Lara-Castro, A.L. Herrera-May, R. Juarez-Aguirre, F. Lopez-Huerta, C.A. Ceron-Alvarez, I.E. Cortes-Mestizo, E.A. Morales-Gonzalez, H. Vazquez-Leal, and S.M. Dominguez-Nicolas, "Portable signal conditioning system of a MEMS magnetic field sensor for industrial applications," *Microsystem Technologies*. vol. 23(1), pp. 215-223, 2017.

[93] W. Chen, K. Hu, and E. Li, "Low-cost land vehicle attitude determination using single-epoch GPS data, MEMS-based inclinometer measurements," *Acta Geodaetica et Geophysica*. vol. 52(1), pp. 111-129, 2017.

[94] A.A. Azab, E.M. El-Menyawy, A.M. Mansour, G.M. Mahmoud, and F.S. Terra, "Structural, Optical and Electrical Properties of Nanocrystalline PbSe: In Films," *Recent Patents on Materials Science*. vol. 11(1), pp. 41-47, 2018.

[95] A.M. Mansour, E.M. El-Menyawy, G.M. Mahmoud, A.A. Azab, and F.S. Terra, "Structural, optical and galvanomagnetic properties of nanocrystalline $Se_{51.43}In_{44.67}Pb_{3.9}$ thin films," *Materials Research Express*. vol. 4(11), pp. 115903, 2017.

[96] A.M. Mansour, "High quality insb microcrystal hall sensor doped with Te or Bi," *International Journal of Advanced Applied Physics Research*. vol. 3(1), pp. 5-10, 2016.

[97] A.M. Mansour, F.S Terra, and A.A Higazy, *Semiconductor-Metal Hybrid Structure (SMHS). Noor Publishing*, Saarbrücken, 2016.

[98] A.M. Mansour, *Semiconductor-meatal hypride structure and pn junctions made from A3B5*. *LAMBERT Academic Publishing*, Berlin, 2015.

[99] F. Terra, A. Higazy, G. Mahmoud, and A. Mansour, "InS semiconductor-metal hybrid structure (SMH) as a magnetic sensor prepared by flash evaporation," *Int. J. Nanoelectronics and Materials*. vol. 3, pp. 53-61, 2010.

[100] F.S. Terra, A.A. Higazy, G.M. Mahmoud, and A.M. Mansour, "(InSb/GaAs)-Au hybrid macro-structure prepared by flash evaporation," *Indian Journal of Physics*. vol. 84(3), pp. 265-277, 2010.

[101] J. Nickel, *Magnetoresistance overview*. *Hewlett-Packard Laboratories Technical Publications Dept.*, Palo Alto Calif., 1995.

[102] Christopher H. Bajorek, *Magnetoresistive (MR) heads and the earliest MR head-based disk drives: Sawmill and Corsair*. , Mountain View, CA, 2014.

[103] Bell Telephone Laboratories, "Permalloy," *Journal of Chemical Education*. vol. 2(12), pp. 1157-1158, 1925.

[104] M.N. Baibich, J.M. Broto, A. Fert, F. Nguyen Van Dau, and F. Petroff "Giant Magnetoresistance of (001)Fe/(001)Cr Magnetic Superlattices," *Physical Review Letters*. vol. 61(21), pp. 2472-2475, 1988.

[105] P.P. Freitas, F. Silva, N.J. Oliveira, L.V. Melo, L. Costa, and N. Almeida, "Spin valve sensors," *Sensors and Actuators, A: Physical*. vol. 81(1), pp. 2-8, 2000.

[106] M.J. Carey, S. Maat, P. Rice, R.F.C. Farrow, R.F. Marks, A. Kellock, P. Nguyen, and B.A. Gurney, "Spin valves using insulating cobalt ferrite exchange-spring pinning layers," *Applied Physics Letters*. vol. 81(6), pp. 1044-1046, 2002.

[107] J.L. Leal, and M.H. Kryder, "Interlayer coupling in spin valve structures," *IEEE Transactions on Magnetics*. vol. 32(5), pp. 4642-4644, 1996.

[108] J.M. Teixeira, J.O. Ventura, R.P. Fermento, J.P. Araujo, J.B. Sousa, S.C. Freitas, and P.J. Freitas, "Interlayer coupling and magnetoresistance of MnIr-Based spin valves: Dependencies on deposition rate, spacer thickness, and temperature," *IEEE Transactions on Magnetics*. vol. 43(7), pp. 3143-3145, 2007.

[109] J.S. Moodera, L.R. Kinder, T.M. Wong, and R. Meservey, "Large magnetoresistance at room temperature in ferromagnetic thin film tunnel junctions," *Physical Review Letters*. vol. 74(16), pp. 3273-3276, 1995.

[110] E.Y. Tsymbal, O.N. Mryasov, and P.R. LeClair, "Spin-dependent tunnelling in magnetic tunnel junctions," *Journal of Physics: Condensed Matter*. vol. 15(4), pp. R109-R142, 2003.

[111] V.K. Varadan, L. Chen, and J. Xie, *Nanomedicine*. *John Wiley & Sons, Ltd*, Chichester, 2008.

[112] G. Korotcenkov, Ed., *Chemical Sensors Simulation and Modeling Volume 5: Electrochemical Sensors. Momentum Press*, New York, 2013.

[113] B. Doudin and M. Viret, "Ballistic magnetoresistance?," *Journal of Physics: Condensed Matter*. vol. 20(8), pp. 083201 (18pp), 2008.

[114] P.F. Schewe, "Ballistic magnetoresistance," *Physics Today*. vol. 55(8), pp. 9, 2002.

[115] S.A. Solin, S.A. Solin, T. Thio, D.R. Hines, and J.J. Heremans, "Enhanced room-temperature geometric magneto-resistance in inhomogeneous narrow-gap semiconductors," *Science*. vol. 289 (5484), pp. 1530-1532, 2000.

[116] J. Moussa, L.R. Ram-Mohan, J.M. Sullivan, T. Zhou, D.R. Hines, and S.A. Solin, "Finite-element modeling of extraordinary magnetoresistance in thin film semiconductors with metallic inclusions," *Physical Review B*. vol. 64(18), pp. 184410, 2001.

[117] J. Sun, C.P. Gooneratne, and J. Kosel, "Design study of a bar-type EMR device," *IEEE Sensors Journal*. vol. 12(5), pp. 1356-1360, 2012.

[118] J. Sun and J. Kosel, "Finite element analysis on the influence of contact resistivity in an extraordinary magnetoresistance magnetic field micro sensor," *Journal of Superconductivity and Novel Magnetism*. vol. 25(8), pp. 2749-2752, 2012.

[119] M. Holz, O. Kronenwerth, and D. Grundler, "Semiconductor-metal hybrid structures as local magnetic-field probes: Magnetoresistance and spatial sensitivity profile," *Applied Physics Letters*. vol. 87(17), pp. 172501, 2005.

[120] M. Holz, O. Kronenwerth, and D. Grundler, "Magnetoresistance of semiconductor-metal hybrid structures: The effects of material parameters and contact resistance," *Physical Review B*. vol. 67(19), p. 195312(10pp), 2003.

[121] M. Holz, O. Kronenwerth, and D. Grundler, "Optimization of semiconductor–metal hybrid structures for application in magnetic-field sensors and read heads," *Applied Physics Letters*. vol. 83(16), pp. 334-3346, 2003.

[122] J. Moussa, L.R. Ram-Mohan, A.C.H. Rowe, and S.A. Solin, "Response of an extraordinary magnetoresistance read head to a magnetic bit," *Journal of Applied Physics*. vol. 94(2), pp. 1110-1114, 2003.

[123] C.H. Möller, O. Kronenwerth, D. Grundler, W. Hansen, C. Heyn, and D. Heitmann, "Extraordinary magnetoresistance effect in a microstructured metal–semiconductor hybrid structure," *Applied Physics Letters*. vol. 80(21), pp. 3988-3990, 2002.

[124] I.S. Ibrahim, V.A. Schweigert, and F.M. Peeters, "Diffusive transport in a Hall junction with a microinhomogeneous magnetic field," *Physical Review B*. vol. 57(24), pp. 15416-15427, 1998.

[125] J. Sun and J.J. Kosel, "Influence of semiconductor/metal interface geometry in an EMR sensor," *IEEE Sensors Journal*. vol. 13(2), pp. 664-669, 2013.

[126] J. Lu, H. Zhang, W. Shi, Z. Wang, Y. Zheng, T. Zhang, N. Wang. Z. Tang, and P. Sheng, "Graphene magnetoresistance device in van der pauw geometry," *Nano Letters*. vol. 11(7), pp. 2973-2977, 2011.

[127] J. Suh, W. Kim, J. Chang, S.-H. Han, and E.K. Kim, "Magneto-resistance of a polycrystalline InSb disk with an embedded Au core," *Journal of the Korean Physical Society*. vol. 55(2), pp. 577-580, 2009.

[128] T.H. Hewett and F. V. Kusmartsev, "Geometrically enhanced extraordinary magnetoresistance in semiconductor-metal hybrids," *Physical Review B - Condensed Matter and Materials Physics*. vol. 82(21), pp. 3-6, 2010.

[129] T.F. Rosenbaum, R. Xu, A. Husmann, M.-L. Saboungi, J.E. Enderby, and P.B. Littlewood, "Large magnetoresistance in non-magnetic silver chalcogenides," *Nature*. vol. 390(6655), pp. 57-60, 1997.

[130] W.R. Branford, A. Husmann, S.A. Solin, S.K. Clowes, T. Zhang, Y.V. Bugoslavsky, and L.F. Cohen "Geometric manipulation of the high-field linear magnetoresistance in InSb epilayers on GaAs (001)," *Applied Physics Letters*. vol. 86(20), pp. 202116, 2005.

[131] S.A. Solin, D.R. Hines, A.C.H. Rowe, J.S. Tsai, and Y.A. Pashkin, "Nanoscopic magnetic field sensor based on extraordinary magnetoresistance," *Journal of Vacuum Science & Technology B: Microelectronics and Nanometer Structures*. vol. 21(6), pp. 3002-3006, 2003.

[132] T. Zhou, D.R. Hines, and S.A. Solin, "Extraordinary magneto-resistance in externally shunted van der Pauw plates," *Applied Physics Letters*. vol. 78(5), pp. 667-669, 2001.

[133] C. bing Rong, H. wei Zhang, J. rong Sun, and B. gen Shen, "Geometry and material optimization of the extraordinary magnetoresistance in the semiconductor-metal hybrid structure," *Journal of Magnetism and Magnetic Materials*. vol. 301(2), pp. 407-414, 2006.

[134] C.-B.B. Rong, H.-W.W. Zhang, J.-R.R. Sun, and B.-G.G. Shen, "Enhanced extraordinary magnetoresistance in the semiconductor-metal hybrid structure with three current leads," *Applied Physics Letters*. vol. 89(5), pp. 3-5, 2006.

[135] M. Hoener, O. Kronenwerth, C. Heyn, D. Grundler, and M. Holz, "Geometry-enhanced magnetoresistance of narrow Au/InAs hybrid structures incorporating a two-dimensional electron system," *Journal of Applied Physics*. vol. 99(3), pp. 2-5, 2006.

[136] Jian Sun, J. Kosel, C. Gooneratne, and Yeong-Ah Son, "Optimization of an Extraordinary Magnetoresistance sensor in the semiconductor-metal hybrid structure," In: *2010 IEEE Sensors*. pp. 1329-1332. *IEEE* (2010).

[137] J. Sun, S.B. Patil, Y.A. Soh, and J. Kose, "Strong temperature dependence of extraordinary magnetoresistance correlated to mobility in a two-contact device," *Applied Physics Express*. vol. 5(3), p. 033002(3pp), 2012.

[138] M. Holz, O. Kronenwerth, and D. Grundler, "Enhanced sensitivity due to current redistribution in the Hall effect of semiconductor-metal hybrid structures," *Applied Physics Letters*. vol. 86(7), pp. 1-3, 2005.

[139] T.D. Boone, N. Smith, L. Folks, J.A. Katine, E.E. Marinero, and B.A. Gurney, "Mesoscopic EMR device magnetic sensitivity in I-V-I-V configuration," *IEEE Electron Device Letters*. vol. 30(2), pp. 117-119, 2009.

[140] J. Sun, and J. Kosel, "Hall effect enhanced low-field sensitivity in a three-contact extraordinary magnetoresistance sensor," *Applied Physics Letters*. vol. 100(23), pp. 1-4, 2012.

[141] M. Oszwaldowski, S. El-Ahmar, and J. Jankowski, "Extraordinary magnetoresistance in planar configuration," *Journal of Physics D: Applied Physics*. vol. 45(14), pp. 145002(6pp), 2012.

[142] A.S. Troup, D.G. Hasko, J. Wunderlich, and D.A. Williams, "Magnetoresistance in silicon-based semiconductor-metal hybrid structures," *Applied Physics Letters*. vol. 89(2), pp. 3-5, 2006.

[143] S.D. Parker, R.L. Williams, R. Droopad, R. Stradling, K. Barnham, S. Holmes, J. Laverty, C. Phillips, E. Skuras, and R. Thomas, "Observation and control of the amphoteric behaviour of Si-doped InSb grown on GaAs by MBE," *Semiconductor Science and Technology*. vol. 4(8), pp. 663-676, 1989.

[144] H. Kroemer, "The 6.1 Å family (InAs, GaSb, AlSb) and its heterostructures: A selective review," *Physica E: Low Dimensional Systems and Nanostructures*. vol. 20(3-4), pp.196-203, 2004.

[145] S. Pisana, P.M. Braganca, E.E. Marinero, and B. a. Gurney, "Graphene magnetic field sensors," *IEEE Transactions on Magnetics*. vol. 46(6), pp. 1910-1913, 2010.

[146] S. Pisana, P.M. Braganca, E.E. Marinero, and B.A. Gurney, "Tunable nanoscale graphene magnetometers," *Nano Letters*. vol. 10(1), pp. 341-346, 2010.

[147] A.L. Friedman, J.T. Robinson, F.K. Perkins, and P.M. Campbell, "Extraordinary magnetoresistance in shunted chemical vapor deposition grown graphene devices," *Applied Physics Letters*. vol. 99(2), pp. 3-5, 2011.

[148] J. Sun, and J. Kosel, "Extraordinary magnetoresistance in semiconductor/metal hybrids: A review," *Materials*. vol. 6(2), pp. 500-516, 2013.